Brain, Behavior, and Immunity 115 (2024) 543–554

Contents lists available at ScienceDirect

Brain Behavior and Immunity

journal homepage: www.elsevier.com/locate/ybrbi

Specific serum autoantibodies predict the development and progression of Alzheimer's disease with high accuracy

Liangjuan Fang [a,b,c,d,e,1], Bin Jiao [a,b,c,d,e,1], Xixi Liu [a], Zhenghong Wang [f], Peng Yuan [g], Hui Zhou [a], Xuewen Xiao [a], Liqin Cao [c,h], Jifeng Guo [a,b,c,d,e], Beisha Tang [a,b,c,d,e], Lu Shen [a,b,c,d,e,*]

[a] Department of Neurology, Xiangya Hospital, Central South University, Changsha, China
[b] National Clinical Research Center for Geriatric Disorders, Central South University, Changsha, China
[c] Engineering Research Center of Hunan Province in Cognitive Impairment Disorders, Central South University, Changsha, China
[d] Hunan International Scientific and Technological Cooperation Base of Neurodegenerative and Neurogenetic Diseases, Changsha, China
[e] Key Laboratory of Hunan Province in Neurodegenerative Disorders, Central South University, Changsha, China
[f] Huadong Hospital Affiliated to Fudan University, Shanghai, China
[g] Department of Rehabilitation Medicine, Huashan Hospital, State Key Laboratory of Medical Neurobiology, Institute for Translational Brain Research, MOE Frontiers Center for Brain Science, Fudan University, Shanghai, China
[h] Hunan Xiansai Institute, Changsha, China

ARTICLE INFO

Keywords:
Alzheimer's disease
Biomarker
Serum autoantibodies
Early detection
Predicting

ABSTRACT

Autoimmunity plays a key role in the pathogenesis of Alzheimer's disease (AD). However, whether autoantibodies in peripheral blood can be used as biomarkers for AD has been elusive. Serum samples were obtained from 1,686 participants, including 767 with AD, 146 with mild cognitive impairment (MCI), 255 with other neurodegenerative diseases, and 518 healthy controls. Specific autoantibodies were measured using a custom-made immunoassay. Multivariate support vector machine models were employed to investigate the correlation between serum autoantibody levels and disease states. As a result, seven candidate AD-specific autoantibodies were identified, including MAPT, DNAJC8, KDM4D, SERF1A, CDKN1A, AGER, and ASXL1. A classification model with high accuracy (area under the curve (AUC) = 0.94) was established. Importantly, these autoantibodies could distinguish AD from other neurodegenerative diseases and out-performed amyloid and tau protein concentrations in cerebrospinal fluid in predicting cognitive decline ($P < 0.001$). This study indicated that AD onset and progression are possibly accompanied by an unappreciated serum autoantibody response. Therefore, future studies could optimize its application as a convenient biomarker for the early detection of AD.

1. Introduction

Alzheimer's disease (AD) is the leading cause of dementia that affects more than 50 million people worldwide (GBD 2019 Dementia Forecasting Collaborators, 2022; Scheltens et al., 2021). However, the exact mechanism underlying its pathogenesis remains unclear. Although many studies have focused on the pathological changes in the central nervous system (CNS) during AD development (Ferrari and Sorbi, 2021; Jack et al., 2018; Sadick et al., 2022), relatively little is known about the changes in the periphery. Recent studies have revealed that there could also be characteristic changes in the periphery, contradicting the notion that AD is a brain-specific disease. For example, plasma levels of 25-OH-vitamin D (Afzal et al., 2014; Nourhashemi et al., 2018), amyloid-β (Aβ) (Chatterjee et al., 2022; Nakamura et al., 2018), different phosphoforms of tau (Ashton et al., 2021; Bayoumy et al., 2021), neurofilament light chain (NFL) (Illán-Gala et al., 2021; Preische et al., 2019), gut microbiome dysbiosis (Angelucci et al., 2019; Sorboni et al., 2022), and immune responses (Bettcher et al., 2021; Sabatino et al., 2019; Wu et al., 2021) have been reported to be associated with the development of AD. Additionally, apolipoprotein E4 (*APOE ε4*), which is the most important genetic risk factor for sporadic AD, induces AD-related neuroinflammation from the periphery (Li et al., 2022). Elucidating peripheral

* Corresponding author at: Department of Neurology, Xiangya Hospital, Central South University, 87 Xiangya Road, Changsha 410000, China.
E-mail address: shenlu@csu.edu.cn (L. Shen).
[1] These authors equally contributed to the work.

https://doi.org/10.1016/j.bbi.2023.11.018
Received 24 April 2023; Received in revised form 13 October 2023; Accepted 16 November 2023
Available online 19 November 2023

changes may provide more insights into the mechanistic understanding of AD.

Among the peripheral changes that occur during AD, we speculated that an autoimmune reaction might provide a specific signature closely accompanied by the disease development. AD significantly disrupts the blood–brain barrier (BBB) integrity and function (Huang et al., 2020; Yarchoan et al., 2012; Zlokovic, 2011). Simultaneously, the neurodegeneration process also generates numerous debris. We argue that AD pathology presents a unique opportunity to expose the immune system to CNS proteins, which would not have been accessible. On the other hand, this enhanced autoimmune response could exacerbate the inflammatory condition in the CNS. Previous studies have found that some autoantibodies in serum were related to AD. Wang et al. identified six AD-associated autoantibodies, including NAP1L3, MAP4, PANK3, PIK3R1, PTP4A1 and SOX15 (Wang et al., 2020). Segundo-Acosta et al. identified a panel of AD-specific autoantibodies against peptides from Anthrax toxin receptor 1, Nuclear protein 1, Glycogen phosphorylase, and Olfactory receptor 8 J1 (San Segundo-Acosta et al., 2019). Segundo-Acosta et al. also identified three serum AD-specific autoantibodies against IVD, ADD2, and CYFIP1, which showed a noticeable AD diagnostic ability (San Segundo-Acosta et al., 2021). However, these studies on autoantibodies related to AD mainly enrolled a limited sample size, besides, whether other new serum autoantibodies exist for AD detection was still unclear.

Consequently, based on the above-mentioned assumption and previous reports (**Supplemental** Table S1), we explored the changes in the level of serum autoantibodies among a large group of participants. We found that a group of seven autoantibodies presented a combinatory signature that showed high specificity and sensitivity in distinguishing patients with AD from healthy controls or those with other neurodegenerative disorders. Interestingly, the autoantibody changes showed close relationships with cognitive decline that provide an opportunity to identify patients with MCI. Therefore, we found that autoimmune responses in the periphery are highly specific to the brain changes of AD, highlighting the potential application of these responses as a minimally invasive tool for early AD detection.

2. Material and methods

2.1. Experimental design

In total, four cohorts were enrolled in this study. The discovery cohort (Cohort 1) comprised patients clinically diagnosed with probable AD (n = 137) and age- and sex-matched healthy controls (n = 133). The validation cohort (Cohort 2) included patients with AD (n = 185), who underwent lumbar puncture, Aβ-positron emission tomography (PET), or AD causative gene (presenilin-1 (*PSEN1*), presenilin-2 (*PSEN2*), and amyloid protein precursor (*APP*)) detection, and were diagnosed using the A + T + N + biological diagnostic framework or pathogenic gene mutation and age- and sex-matched healthy controls (n = 130). Additionally, the expanded validation cohort (Cohort 3) was from the Cognitive Impairment Multicenter Database and Collaborative Network in China (CI-MDCNC), which includes patients with clinically diagnosed probable AD (n = 445) and MCI (n = 146) who carried at least one *APOE ε4* allele, and age- and sex-matched healthy controls (n = 255). Furthermore, the differential diagnosis cohort (Cohort 4) comprised patients (n = 255) with other neurodegenerative diseases. Patients and healthy controls were enrolled from the Department of Neurology, Xiangya Hospital, Central South University for Cohorts 1, 2, and 4. Patients with MCI, AD, frontotemporal dementia (FTD), dementia with Lewy bodies (DLB), progressive supranuclear palsy (PSP), and Parkinson's disease (PD) were diagnosed based on their respective criteria (Albert et al., 2011; Höglinger et al., 2017; McKeith et al., 2005; McKhann et al., 2011; Postuma et al., 2015; Rascovsky et al., 2011). All patients with AD underwent detailed clinical and cognitive evaluations without comorbidities like auto-immune disease, cardiovascular disease, cerebrovascular diseases, diabetes etc. The study protocol was approved by the Institutional Review Board of Xiangya Hospital of Central South University in China. Written informed consent was obtained from each participant or their guardian.

2.2. Core biomarkers measurements in cerebrospinal fluid (CSF)

In Cohort 2, CSF of patients with AD was collected by lumbar puncture according to international guidelines (Seeburger et al., 2015) and used to test for four core biomarkers (i.e., Aβ42, Aβ40, total tau (t-tau), and phosphorylated tau (p-tau)). First, the samples were centrifuged at 2000 × g at 4 °C for 10 min and stored at −80 °C. Next, CSF biomarkers were assessed using an enzyme-linked immunosorbent assay (ELISA) (Cat. No. EQ 6511–9601, EQ 6521–9601, EQ 6591–9601, EQ 6531–9601; EUROIMMUN, Germany) and performed by experienced technicians in strict accordance with the instructions of the manufacturer (Teunissen et al., 2009).

2.3. PiB-PET acquisition and interpretation

^{11}C-labelled Pittsburgh compound-B (PiB) PET imaging were performed and analyzed as previously described (Lopresti et al., 2005). Briefly, images were acquired 50 min after PiB was injected intravenously (12 mCi, 1 Ci/μmol, over 20 sec). The examinations were performed by qualified Nuclear Medicine Technologists. Cortical regions exhibiting the most distinct radiotracer accumulation in Aβ-positive subjects typically include lateral temporal, frontal lobes, posterior cingulate cortex/precuneus, and the parietal lobes, whereas the sensorimotor cortex and the visual cortex can be relatively spared (Minoshima et al., 2016). The cerebellum was used as a reference region for visual interpretation. The results were interpreted by three experienced nuclear medicine physicians who complete appropriate training programs provided by the manufacturer of radiotracer.

2.4. Gene analysis

Genomic DNA was extracted from the peripheral blood leukocytes of patients with AD using the QIAGEN kit, following the manufacturer's instructions. In Cohort 2, 33 patients with AD with pathogenic or probable pathogenic variants in *PSEN1*, *PSEN2*, or *APP* were enrolled, as reported in the previous studies (Jiao et al., 2021). Additionally, all patients with MCI and AD in Cohort 3 had at least one *APOE ε4* allele. Polymerase chain reaction (PCR) for *APOE* genotyping was performed using the previously reported primers, and each PCR product was sequenced using an ABI 3730xl DNA analyzer (Jiao et al., 2014).

2.5. Production of recombinant antigens for autoantibody assays

Candidate autoantigens related to AD were selected based on previous studies (**Supplemental** Table 1). The full-length cDNA and cDNA fragments corresponding to various domains of each protein were amplified by PCR as previously described (Daniilidou et al., 2011). The different domains of each protein were selected using Uniprot software (https://www.uniprot.org/). The antigen peptide distributions were analyzed using IEDB software (https://www.iedb.org). The exposure of epitopes and hydrophily were analyzed using DNASTAR software (https://www.dnastar.com). The three-dimensional structure of proteins and fragments were constructed using PYMOL software (https://pymol.org/2/). The PCR fragments were digested with the respective endonucleases, repurified and subcloned into the respective sites of the bacterial expression vector and expressed (Fig. 1). Briefly, primers were designed using a human cDNA library (Invitrogen) or whole gene synthetic DNA as a template, and the full-length genes or cDNA fragments of the candidate proteins were cloned into the pET28 expression vector using molecular cloning methods such as PCR, enzyme digestion, and ligation. Simultaneously, tags, including His and c-myc, were added at

Table 1
Characteristics of 1686 participants enrolled in this study.

	Cohort 1 (n = 270)		Cohort 2 (n = 315)		Cohort 3 (n = 846)			Cohort 4 (n = 255)			
	AD (n = 137)	Control (n = 133)	AD (n = 185)	Control (n = 130)	MCI (n = 146)	AD (n = 445)	Control (n = 255)	DLB (n = 44)	FTD (n = 71)	PSP (n = 52)	PD (n = 88)
Age, years	63.55 (9.47)	64.98 (7.62)	59.55 (9.01)	60.82 (5.70)	66.21 (9.45)	67.18 (9.94)	65.56 (7.79)	72.41 (7.58)	62.31 (9.84)	64.79 (7.70)	63.90 (11.94)
Sex, Male, %	38	32.3	47	45.4	40.4	36.9	43.1	68.2	45.1	55.8	43.5
ADO, years	60.92 (9.75)		56.66 (9.01)		63.62 (9.59)	64.21 (10.04)		70.72 (7.97)	59.66 (9.76)	62.13 (7.85)	53.97 (10.39)
COD, years	2.63 (2.06)		2.87 (2.09)		2.59 (2.29)	2.97 (2.43)		2.38 (1.76)	2.64 (1.90)	2.66 (1.48)	7.47 (4.80)
Education, years	9.13 (4.44)	8.19 (3.90)	9.57 (3.91)	8.83 (2.29)	9.48 (4.16)	9.76 (4.05)	8.55 (1.78)	8.18 (2.62)	9.08 (3.80)	7.33 (3.63)	7.72 (2.85)
MMSE	14.62 (7.00)	28.02 (0.88)	12.75 (7.06)	28.79 (1.17)	25.91 (3.21)	13.62 (6.40)	28.80 (0.65)	17.41 (2.94)	18.66 (2.53)	21.31 (3.12)	21.35 (3.59)
MoCA	9.91 (5.29)	27.53 (0.97)	8.05 (5.72)	27.98 (1.12)	19.57 (6.30)	9.03 (5.05)	27.95 (1.05)	13.27 (3.87)	15.76 (4.53)	15.87 (3.55)	18.78 (5.44)
CDR	1.47 (0.86)		1.84 (0.84)		0.47 (0.12)	1.77 (0.74)		1.64 (0.65)	1.35 (0.75)		
NPI	17.6 (14.71)		18.47 (17.302)		8.48 (9.66)	18.04 (14.92)		25.55 (9.30)	24.25 (12.76)	2.54 (2.16)	2.67 (1.87)
ADL	31.6 (10.13)		35.19 (12.238)		21.85 (2.94)	33.34 (11.00)		36.61 (7.85)	30.17 (4.96)	29.52 (5.59)	29.78 (4.89)
CSF Aβ42, pg/ml			409.38 (212.01)								
CSF Aβ40, pg/ml			7704.95 (6498.66)								
CSF Aβ42/40			0.06 (0.03)								
CSF p-tau181, pg/ml			102.66 (115.75)								
CSF t-tau, pg/ml			417.97 (335.48)								

Data are mean (SD) or n (%). ADO, Age of disease onset; COD: course of disease; MMSE, Mini-Mental State Examination; MoCA, Montreal Cognitive Assessment; CDR, Clinical Dementia Rating Scale; NPI, neuropsychiatric inventory; ADL, Activity of Daily Living Scale. In cohort 1, 2, 3, the cases and controls were matched with age and sex.

the N-terminus of the protein to form a fusion protein. Next, the recombinant expression vector was identified through DNA sequencing to confirm the correct gene sequence. Recombinant proteins were expressed in *E. coli* BL21/DE3 cells (Novagen). Briefly, cells were grown aerobically at 37 °C, and 200 rpm in lysogeny broth (LB) (Difco) supplemented with 50 μg/ml kanamycin overnight. Next, the target gene expression was induced by adding 0.1 mM isopropyl-β-d-thiogalactopyranoside (IPTG) at an OD600 of ~ 0.8. The recombinant protein was purified using Ni2 + affinity chromatography and gel-filtration chromatography. Subsequently, the molecular weight and purity of the target proteins were determined using sodium dodecyl sulfate–polyacrylamide gel electrophoresis (SDS-PAGE). The concentration of each target protein was determined using the Bradford assay. Finally, the purified antigens were aliquoted and stored at −80 °C.

2.6. ELISA procedure

First, we fixed the purified candidate proteins or myc as positive control on the bottom of the tissue culture plates and quantified the concentrations of serum antibodies in a blinded manner. Briefly, the purified recombinant and control proteins were diluted and coated onto the surfaces of 96-well plates overnight at room temperature. After washing in phosphate-buffered saline containing 0.1 % Tween 20 (pH 7.6) and blocking with casein blocking buffer, the serum samples (diluted 1:110 in blocking buffer) or anti-myc antibody were added to the reagent wells and shaken at room temperature for 60 min. Next, following the manufacturer's instructions, horseradish peroxidase (HRP)-conjugated anti-human IgG antibody (BD Biosciences, 555788) and substrate solutions were added serially after incubation and washing. Each well's optical density (OD) was measured spectrophotometrically at a wavelength of 450 nm. Subsequently, we performed three technical replicates on samples and standards and used the average value of the replicate for downstream statistical analyses. The cut-off level for positive reactions was defined as the mean plus two standard deviations of the OD reading in healthy controls samples. Data are presented as the mean OD corrected for background noise (wells without coated antigen). Serum samples were interpreted as positive for autoantibodies presence if they displayed a dose–response curve to the antigen titration series and had a signal above the accepted cut-off point. Additionally, we tried different combinations; to further minimize the detection variability, we tested different peptide fragments from each protein and selected the fragment with the most consistent performance.

2.7. Support vector machine (SVM) classification

Raw serum measurements were regressed against age and sex. Each residual serum biomarker was subsequently used for the SVM training. Additionally, the sample size for each class was balanced to minimize bias for each model. In the case of a significantly higher number of participants in one class, a random subset was drawn for the model training and testing, and the processes were repeated to obtain an average performance. Next, for each round of training, 20 % of the data were randomly selected from each class as the testing (holdout validation) group, while the remaining 80 % were fitted to an SVM classifier. Conversely, in the case of multiple classes, multiple binary models were trained in a one-versus-one coding design, as implemented in the error-correcting output code model in MATrix LABoratory (MATLAB). The Gaussian kernel function was applied in all models because preliminary exploration showed superior performance. Within the training set, we applied a 5-fold cross-validation during the training and optimized 'BoxConstraint' and 'KernelScale' in the fitting process to adjust the hyperparameters and regularization. Subsequently, we calculated the model predictions for the testing group to assess the model's performance. Furthermore, we randomly shuffled the class labels in the testing group and recalculated the model prediction accuracy following the predictions for the testing group. This approach enables us to estimate

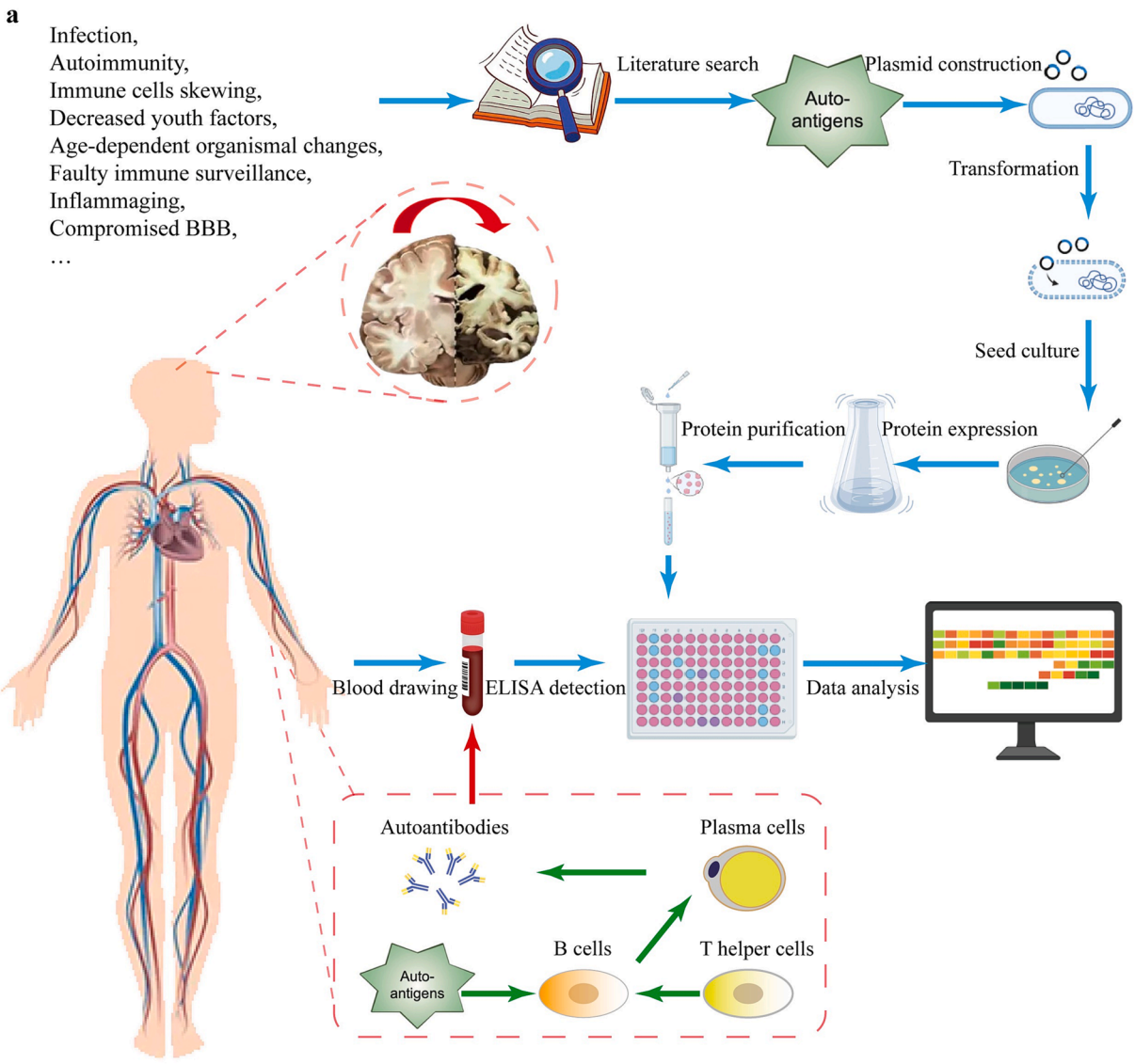

Fig. 1. Schematic flowchart and four datasets in this study. (**A**), schematic of the flowchart. AD is characterized by complex and heterogeneous pathophysiology. Among the peripheral changes during AD, we speculated that an autoimmune reaction might provide a specific signature closely associated with the disease progression. The autoantigens related to AD were selected and expressed based on previous studies. Peripheral blood containing autoantibodies was obtained from the patients and healthy controls. Specific serum autoantibodies were measured using ELISA, and the data were subsequently analyzed. (**B**), number of patients in the four datasets. * The two cohorts shared the healthy control group since we performed ELISA tests on the two cohorts simultaneously. AD, Alzheimer's disease; MCI, mild cognitive impairment; PD, Parkinson's disease; FTD, frontotemporal dementia; DLB, dementia with Lewy bodies; PSP, progressive supranuclear palsy; CI-MDCNC, cognitive impairment multicenter database, and collaborative network in China.

the chance prediction level while maintaining the statistical structure of the dataset. More than 10,000 times of random subsampling of the training and testing groups were calculated to obtain the average performance. Additionally, more than 200 random shuffles are calculated for each model. All calculations and the statistical analyses were performed using MATLAB (R2021b) and GraphPad Prism (v9.0), respectively.

2.8. Partial dependence plot

Partial dependence plot (PDP) utilizes the idea of marginal effect to measure the predictive values of one or two features in a machine learning model. Individual Conditional Expectation (ICE) is a local model-agnostic method deriving from PDP and plots one line for each instance sample separately. ICE value for a line (and one instance

sample) is computed as follows: (1) All predictor features other than the interested one are held the same as actual values; (2) Variants of the instance sample in question are created; (3) Predictions are implemented for these generated variants and the serial outcome values constitutes the ICE line for the relevant instance sample. The computation procedure repeats for each instance sample with respect to a predictor feature of interest. An ICE result is therefore a set of plots, each of which depicts how response value changes as the specified instance sample's value of an interested predictor feature of changes. ICE and PDP are realized in software MATLAB via built-in function Partial Dependence.

2.9. Local interpretable model-agnostic Explanation analysis

Local Interpretable Model-agnostic Explanation (LIME) is a method that interprets criteria on individual predictions of any black-box classifier or regressor by training a surrogate model to approximate the local structure of the black box which underlies the certain prediction. The interpretable model is trained on perturbed samples generated in the neighborhood of a query point concerning the individual prediction. The support vectors of the SVM model were assigned as query points for LIME, which fitted a simple linear model for each support vector to approximate the local structure of the hyperplane. The technique LIME was realized in software MATLAB via built-in function lime.

3. Results

3.1. Demographic characteristics

Table 1 summarizes the demographic information of all patients (n = 1168) and controls (n = 518) in the four cohorts. Pathogenic or likely pathogenic variants of *PSEN1*, *PSEN2* and *APP*, as well as *APOE* genotypes in Cohort 2 were shown in **Supplemental Table S2 and S3.**

3.2. Identification of seven serum autoantibodies

A total of 20 autoantibodies were detected in the serum from Cohort 1 and the concentrations were shown in **Supplemental Figure S1 and Table S4**. Among them, the seven proteins showed the most robust performance with significantly different enrichment between AD patients and healthy controls, including microtubule-associated protein tau (MAPT), DnaJ homolog subfamily C member 8 (DNAJC8), lysine-specific demethylase 4D (KDM4D), small EDRK-rich factor 1A (SERF1A), cyclin-dependent kinase inhibitor 1 (CDKN1A), advanced glycosylation end product-specific receptor (AGER), and polycomb group protein ASXL1 (ASXL1). To further minimize the detection variability, we tested different peptide fragments from each of the seven protein and selected the fragment with the most consistent performance, which includes clone numbers 90F, 94E, 95D, 132A, 2801, 4203, and 8601 of MAPT, DNAJC8, KDM4D, SERF1A, CDKN1A, AGER, and ASXL1, respectively (**Supplemental Materials**). Quantification of the raw serum measurements of the seven autoantibodies in Cohort 1, 2 and 3 were shown in **Supplemental Figure S2.**

3.3. Robust classification ability using combinatorial measurements of seven serum autoantibodies

After identifying seven autoantibodies as the candidate biomarkers for AD in Cohort 1, we tested their performance in identifying patients with AD. We recruited 185 patients with AD according to ATN guidelines and 130 healthy controls in Cohort 2. We measured the levels of the seven autoantibodies in these participants; we found that while all seven indicators showed trends of differential levels in AD and healthy controls consistent with results from initial screening, five (#90F, #94E, #132 A, #2801, and #4203 peptides from MAPT, DNAJC8, SERF1A, CDKN1A, and AGER, respectively) were statistically significant (Fig. 2**A**). While the differences between AD and control group appeared to be slightly less significant than those measured in Cohort 1, all seven measurements showed some degree of separation between patients with AD and healthy controls using the levels of individual serum autoantibodies (Fig. 2**B**).

We then explored whether a combined approach could yield a superior classification performance. We projected seven measurements from all participants in 2-dimensional axes using the t-distributed stochastic neighbor embedding (t-SNE) method (Fig. 2**C**). We found an obvious separation between patients with AD and healthy controls in this reduced plane, which suggests that group-specific information exists in the high-dimensional space in these seven measurements. Subsequently, we further explored a potential classification model using this dataset. We trained an SVM model using the first two principal components of the seven measurements. This approach enabled us to calculate the full parameter space and plot the decision boundary (Fig. 2**D**), which provided an intuitive visualization regarding how the model decided the classification. The model produced high classification accuracy (area under the curve (AUC) = 0.94), which is superior to each measurement alone. Notably, the decision boundary showed a clear nonlinear pattern, suggesting that the combined classification with nonlinear models could be a promising approach to differentiate AD patients from healthy controls.

Based on the findings described above, we formally tested the seven autoantibodies' classification performance using a Gaussian kernel function based SVM model. We constructed 5-fold training and testing subsets from the data and employed a 5-fold cross-validation within the training set for hyperparameter optimization. We obtained an average prediction accuracy of approximately 80 % in the testing group after 10,000 rounds of random subsampling, while the chance-level accuracy was 50 % ($P < 0.0001$, Fig. 2**E**). We further plotted the probability of each participant being classified as having AD or healthy controls among the testing rounds and found robust classification performance across all random subsamples (Fig. 2**F**), which suggests a stable hyperplane that separates patients with AD and healthy controls identified by the SVM models. These data demonstrated a high performance of the combinatorial model using seven antibodies in separating AD from control group.

Moreover, we further examined the combinatorial nature of our SVM models since the contribution of individual autoantibodies to the classification is difficult to interpret because of the nonlinearity in the Gaussian kernel function. To this end, we calculated each serum autoantibody level's individual conditional expectation (ICE) using a representative SVM model (Fig. 2**G**). Notably, these plots display several nonlinear relationships between the prediction scores and serum autoantibody levels, suggesting that the model cannot decide the class using binarized "high" or "low" thresholds. Additionally, to further quantify this nonlinearity, we performed a local interpretable model-agnostic explanatory analysis for each serum autoantibody (Fig. 2**H**). Coefficients β of plasma autoantibody levels in each fitted linear model were illustrated in Fig. 2**H**. Consistent with the ICE plots, we found high variability in the local coefficients. Interestingly, some autoantibodies showed a high impact on the prediction scores despite poor separation between groups alone, indicating that the classification model not only considered the values from individual antibodies but also the correlation between different features.

3.4. Measurements of the seven autoantibodies can reflect cognitive impairment among AD

The above analysis demonstrated the high performance of separating patients with AD and healthy controls using the combined measurements of the seven autoantibodies. A critical yet unresolved issue is whether this combinatorial model acts simply as a biomarker or whether it can identify some key factors that are mechanistically linked with disease progression. Therefore, to explore these two possibilities, we performed a canonical correlation analysis (CCA) between the seven

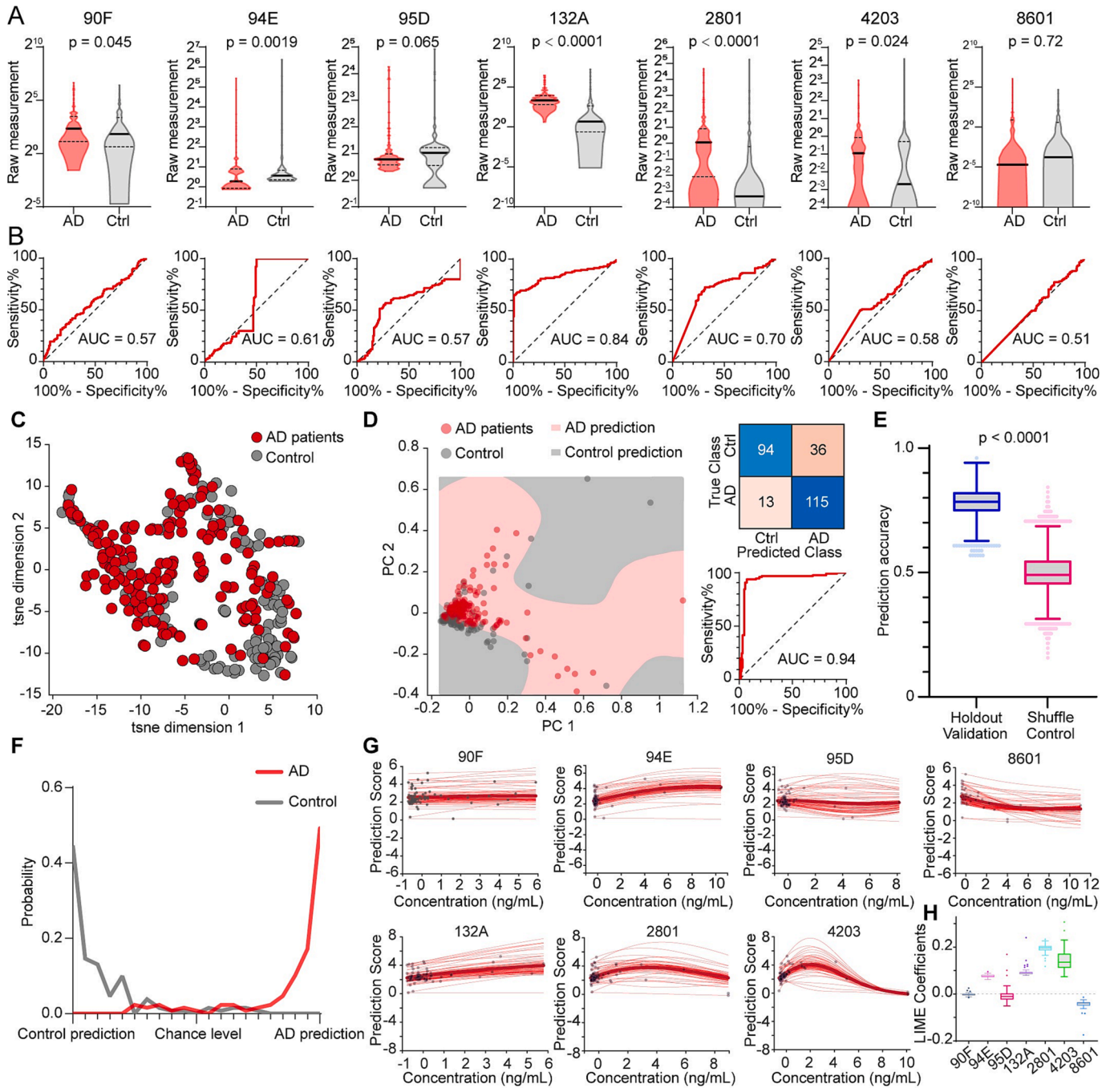

Fig. 2. Robust classification between patients with AD and healthy controls with the levels of serum autoantibodies using the support vector machine. (**A**), level distributions of seven serum autoantibodies among patients with Alzheimer's disease (AD) (Cohort 2, N = 185) and healthy controls (Cohort 2, N = 130). Violin plots show the minimum, first quartile (Q1), median, third quartile (Q3), and maximum values. (**B**), receiver operating characteristic (ROC) curves and corresponding areas under the curve (AUC) for the univariate classification of AD and healthy controls using each serum biomarker alone. (**C**), visualization of the seven serum autoantibody levels in patients with AD and healthy controls using t-distributed stochastic neighbor embedding (t-SNE). (**D**), a representative support vector machine (SVM) model for classifying patients with AD and healthy controls using the first two principal components (PC) of the seven serum autoantibody levels. The model classification results were projected onto the entire parameter range of the PC space. Inserts show the confusion matrix and ROC curves for the performance of AD and healthy control classifications. (**E**), quantification of the performance of the SVM classification for AD and healthy controls using all seven serum biomarkers [Cross-validation group (20000 models); each validation model (200 shuffle controls)]. (**F**), probability distribution of the model prediction score for each patient among the models shown in (E). (**G**), partial dependence plots (PDP) for each serum autoantibody in the best performing SVM model. Each dot represents a support vector patient in the model, and the connecting line shows the corresponding individual conditional expectation (ICE) plots within each predictor feature. (**H**), representation of coefficients of the simple linear model fitted by LIME whose query points are assigned as all support vectors of the SVM model. The coefficient illustration is stratified by the serum autoantibodies, which serve as predictor variables in the surrogate linear model of LIME. The data are exhibited via box-and-whisker plots involving minimum, the first quartile (Q1), median, the third quartile (Q3) and maximum values regardless of outliers, and outliers, where the minimum and the maximum are defined as [Q1 – 1.5*(Q3 – Q1)] and [Q3 + 1.5*(Q3 – Q1)], respectively.

serum autoantibodies and levels of amyloid and tau in the CSF from patients with AD and also their cognitive status (Fig. 3**A**), this method allowed us to extract correlated modes between groups containing multiple variables. Notably, we detected several modes with a high correlation. Mode #2 primarily comprised the patients' cognitive scores, suggesting that measurements of the seven autoantibodies contain information correlated with the patient's cognitive impairment.

Next, we examined the sensitivity of the seven autoantibodies to patients' cognitive scores. Thus, we first established a data-driven approach to cluster the patients into different severity groups. Specifically, we performed a principal component analysis (PCA) of the patient's clinical assessment of the Mini-Mental State Examination (MMSE), Montreal Cognitive Assessment (MoCA), the activity of daily living (ADL), clinical dementia rating (CDR), and neuropsychiatric Inventory (NPI) scores. Interestingly, we found that the first principal component (PC) covered more than 80 % of the total variance, indicating that this PC would most likely align with patients' cognitive status. Additionally, three obvious peaks in the distribution were observed, which were fitted to a 3-term Gaussian curve when we plotted the distribution of the first PC scores from all patients (Fig. 3**B**). Based on this, we categorized the patients with AD into mild, moderate, and severe groups. Furthermore, we retrospectively plotted the cognitive scores in these groups to verify the validity of this staging approach and found significant differences between them as we expected (Fig. 3**C**).

Following the grouping process described above, we analyzed the CSF levels of amyloid, tau, and seven serum autoantibodies in each group. We found lower Aβ42 and higher p-tau levels in the severe group; however, these results were not significant (Fig. 3**D**). Additionally, we used a similar SVM approach to test whether a combined approach of these CSF measurements could provide a better correlation to patients' cognitive status and found that the performance of classifying the mild and moderate groups was only ~ 5 % above the chance level (Fig. 3**E**). In contrast, the measurements of the seven autoantibodies provided much higher accuracy that distinguished the mild group from the moderate group (Fig. 3**E and 3F**). These data strongly indicated that the seven autoantibodies contained information that correlated with the patient's cognitive status.

3.5. *Early detection of prodromal cognitive impairment with the seven serum autoantibodies*

The intriguing fact that measurements of the seven autoantibodies contain information related to cognition suggests that the decision hyperplane employed in our combinatorial SVM model may be aligned with cognitive status. Following this hypothesis, we predict that the SVM model we derived can be generalized across different cohorts and can detect early cognitive impairment even before the patient reaches the clinical criteria for AD. Therefore, to test these predictions, we recruited an expanded-validating cohort (Cohort 3) based on cognitive status, which includes 445 and 146 patients with AD and MCI, respectively, and 255 healthy controls.

We first trained and tested a classification model using seven autoantibodies with the same combinatorial SVM approach. Interestingly, consistent with Cohort 2, we found robust classification accuracy using data acquired from Cohort 3 (~75 % testing accuracy; Fig. 4**A**). Additionally, to test our prediction regarding the generalization between cohorts, we first compared the geometries of the support vectors used in the models in these two cohorts. We found that the two groups of support vector population vector angles to a fixed standard vector were similar; however, random sampling from the same parameter space showed significantly different angles (Fig. 4**B**). This result suggests that the decision hyperplane derived from the two cohorts shared a similar geometry in high-dimensional space, which is consistent with our prediction. Furthermore, we directly tested the cross-cohort performance of the two models. A strong correlation was observed between the predictions from two models (Fig. 4**C**). Moreover, using the prediction

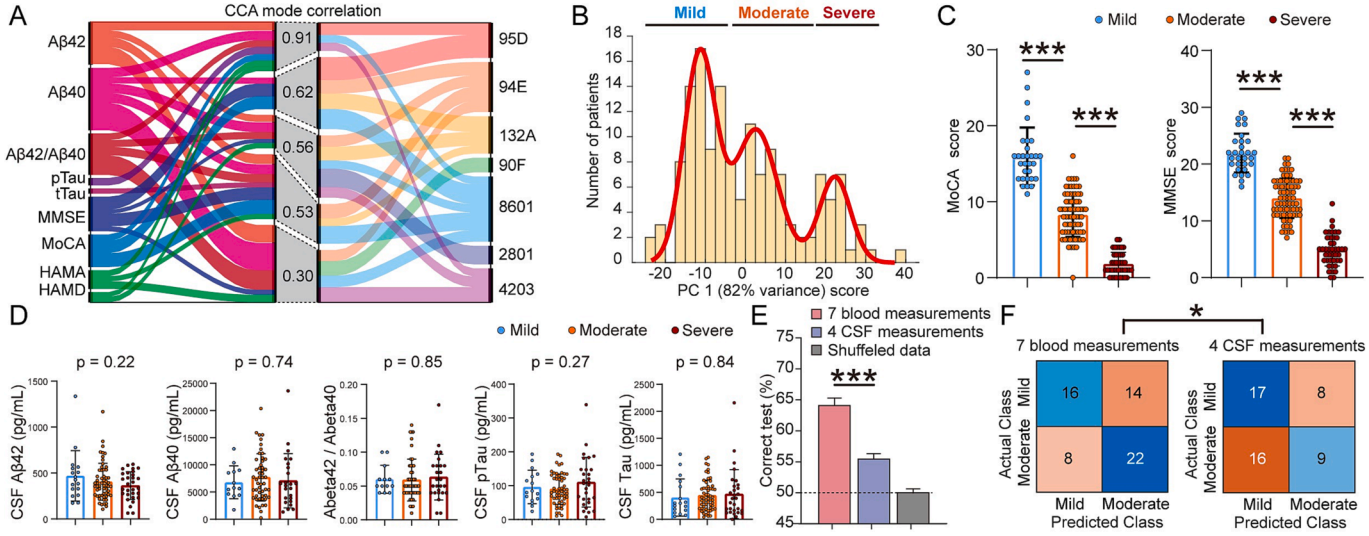

Fig. 3. Serum levels of autoantibodies reflect cognitive variables among patients with AD. Indicate figure parts with bold capital letters: (**A**), Sankey plot for canonical correlation analysis (CCA) depicting the relationships between serum biomarkers and indicators of amyloid-β (Aβ)42, Aβ40, Aβ42/Aβ40, phosphorylated tau (p-Tau), and total tau (t-Tau) in the cerebrospinal fluid (CSF) and clinical assessment of the Mini-Mental State Examination (MMSE), Montreal Cognitive Assessment (MoCA), Hamilton Anxiety Rating Scale (HAM-A), and Hamilton Depression Rating Scale (HAM-D). The correlation coefficients for each mode are labelled in the middle column. (**B**), histogram of cognitive status in patients with Alzheimer's disease (AD), summarized with the first principal component by principal component analysis (PCA) of the clinical assessment of the MMSE, MoCA, activity of daily living (ADL), clinical dementia rating (CDR), and neuropsychiatric Inventory (NPI) scores. The red curve indicates a Gaussian curve fitted to the distribution. The three peaks in the curve were designated severe, moderate, and mild. (**C**), Quantification of MoCA and MMSE scores in different severity groups of patients with AD. The Student's *t*-test was used to compare the groups. (**D**), Quantification of the levels of Aβ42, Aβ40, Aβ42/Aβ40, p-Tau, and t-Tau in the CSF of patients with AD of different severities. The Student's *t*-test was used to compare the groups. (**E**), Quantification of the support vector machine (SVM) model performance in classifying patients with AD with different severities using seven serum autoantibodies or four CSF biomarkers (Aβ42, Aβ40, p-Tau, and t-Tau) as predictors. N = 1000 models for cross-validation. The Student's *t*-test was used to compare the groups. (**F**), Representative confusion matrices of the SVM models from (E). The chi-square test was used to compare the performance. *: $P < 0.05$; **: $P < 0.01$; ***: $P < 0.001$.

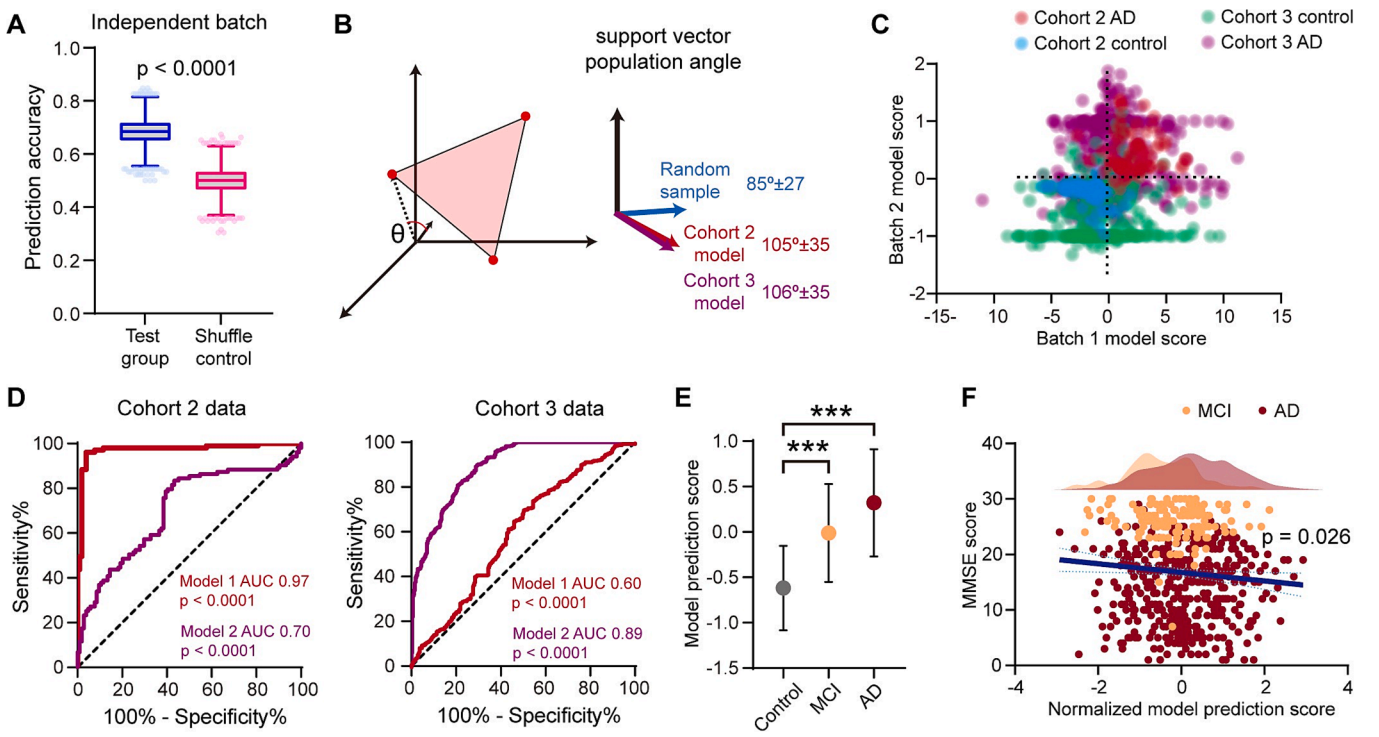

Fig. 4. Serum autoantibodies detect early cognitive decline. (**A**), quantification of the support vector machine (SVM) model performance in classifying Alzheimer's disease (AD) and healthy controls in a separate independent batch of patients. The model was trained and tested using data from Cohort 3 (N = 8000 models for cross-validation and each model corresponded to 100 shuffle controls). Box-and-whisker plots show the values of the first quartile (Q1), median, third quartile (Q3), [Q1 − 1.5 × (Q3 - Q1)], [Q3 + 1.5 × (Q3 - Q1))], and the outliers < [Q1 − 1.5 × (Q3 - Q1)] or > [Q3 + 1.5 × (Q3 - Q1)]. (**B**), population vector angles of the support vectors in the SVM model from Cohort 3 and the model derived from Cohort 2, as described in Fig. 2. (**C**), scatter plot of the two models' prediction scores from Cohorts 2 and 3. (**D**), receiver operating characteristic (ROC) curves for within- and cross-batch model performance. Each curve was compared to the chance level (dotted line) to calculate *P*-values. (**E**), quantification of the model prediction scores in patients with AD, healthy controls, and those with mild cognitive disorders (MCI). The SVM model was trained without the MCI data, as described in (A). Data are presented as mean ± standard deviation. Student's *t* test $^{***}P < 0.001$. (**F**), cloud and rain plot for the Mini-Mental State Examination (MMSE) scores and rank-transformed model prediction scores in the AD and MCI groups. The blue line indicates linear regression analysis including all patients, dotted lines indicate the 95 % confidence interval. The *P*-value indicates the estimated slope of the line compared with 0.

scores from the two models, both cohorts showed significantly higher than chance-level accuracy based on the receiver operating characteristic (ROC) curves (Fig. 4**D**). These data indicated consistent performance of the autoantibodies-based model across different batches.

Subsequently, we calculated the model prediction scores for the clinically identified patients with MCI. On average, the MCI group had significantly higher prediction scores than the control group and lower scores than the AD group (Fig. 4**E**). This gradient effect was impressive to us since the MCI group data were excluded from the model's training set; the consistent trend between cognitive impairment and model prediction score strongly suggested that the decision hyperplane derived from the seven autoantibodies is aligned with the cognitive decline progression in AD. We examined the correlation between the prediction scores (transformed to a normal distribution based on rank) and cognitive status at the individual level to further illustrate the biological relevance of the prediction scores (Fig. 4**F**). Despite the high variability, we observed a significant correlation between the prediction scores and cognitive decline. In summary, these results are consistent with our prediction that the SVM model derived from the seven autoantibodies can be generalized across different cohorts; the model identifies cognitive decline at the early stage as well as during the disease progression.

3.6. The seven serum autoantibodies could distinguish AD from other neurodegenerative disorders

Although the above data demonstrate a high degree of correlation between the seven autoantibodies and cognitive impairment in AD, whether such a correlation is specific to AD development is yet to be determined. Therefore, we investigated the performance of the seven autoantibodies in patients with other neurodegenerative diseases included in Cohort 4 to answer this question. First, we compared AD with PD by visualizing the levels of the seven autoantibodies in a reduced plane (Fig. 5**A**). Patients with PD exhibited a pattern distinct from those with AD and the healthy controls. Subsequently, we quantified the population vector distances and angles in the 7-dimensional space and found significant differences between AD and PD (Fig. 5**B and C**). Following this finding, we constructed a 3-way SVM classifier for AD, PD, and healthy controls using the seven autoantibody measurements. Notably, the model showed high accuracy for each group (Fig. 5**D and E**), which indicates that the information used to separate patients with AD and the healthy controls was specific to these two groups and did not overlap with those with PD.

Finally, we expanded this analysis and examined the measurements of the seven autoantibodies by constructing classifier models for each pair of AD and other neurodegenerative diseases, including PD, FTD, DLB, and PSP. The corresponding ROC curves indicated that the serum biomarker panel could distinguish AD from PD (AUC = 0.91), FTD (AUC = 0.71), and DLB (AUC = 0.55), rather than PSP (AUC = 0.37) (Fig. 5**F**).

Collectively, these data provide the first evidence that serum autoantibodies contain AD-specific information and can accurately reflect disease progression in patients with AD.

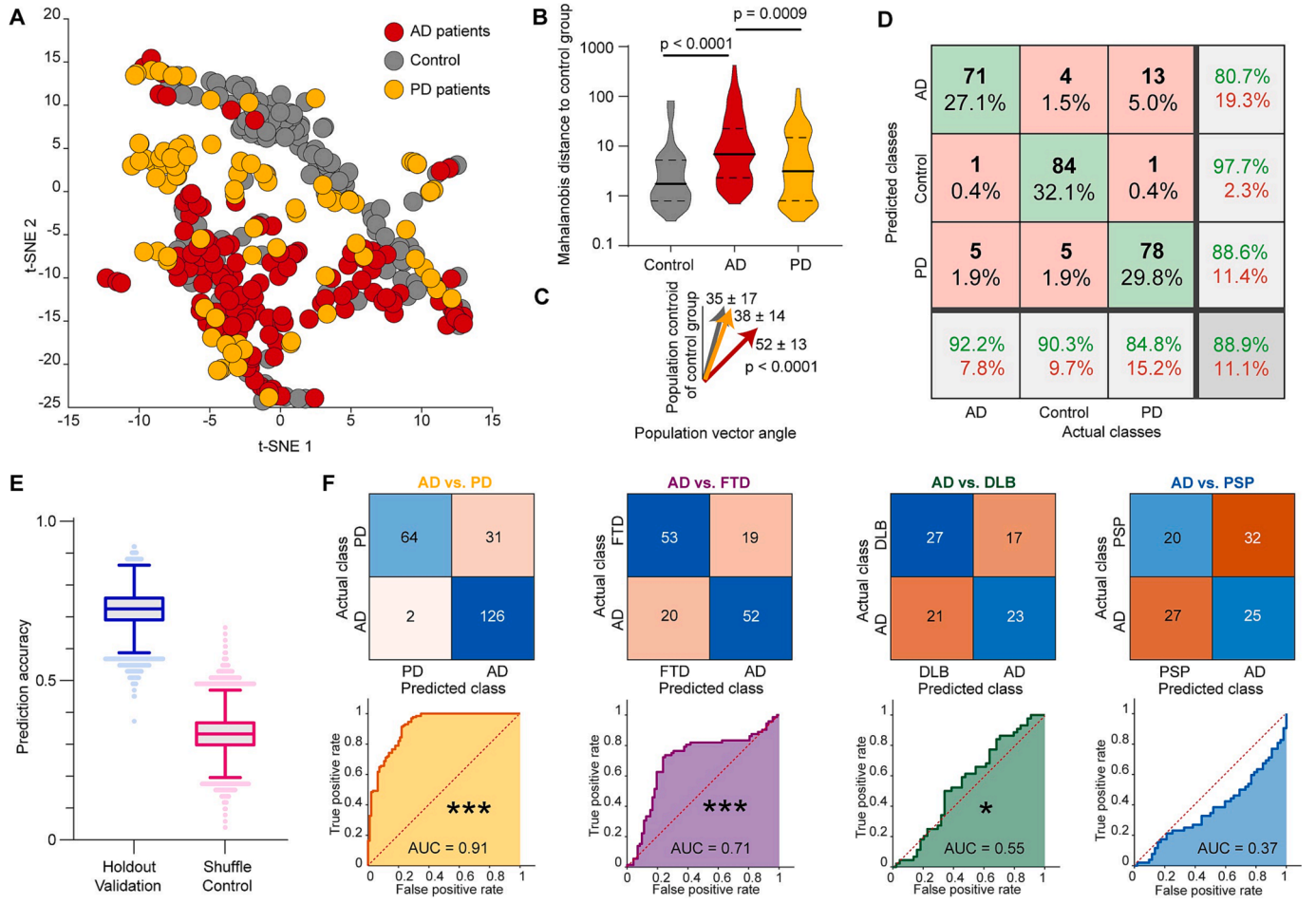

Fig. 5. The levels of serum autoantibodies distinguish patients with AD from other neurodegenerative diseases. (**A**), visualization of seven serum autoantibody levels in Alzheimer's disease (AD), Parkinson's disease (PD), and healthy controls using t-distributed stochastic neighbor embedding (t-SNE). (**B**), quantification of the population vector distances of each patient's serum autoantibody levels compared with those of healthy controls. Student's *t*-test was used to compare the groups. (**C**), similar to (B), calculates the population vector distances. (**D**), representative confusion matrix showing the three-way classification for AD, PD, and healthy controls using the levels of the seven serum autoantibodies as predictors in the support vector machine (SVM) models. (**E**), quantification of three-way model performance for classifying AD, PD, and healthy controls (N = 10 000 models for cross-validation, with each model corresponding to 10,000 shuffle controls). Box-and-whisker plots show the values of the first quartile (Q1), median, third quartile (Q3), [Q1 − 1.5 × (Q3 - Q1)], [Q3 + 1.5 × (Q3 - Q1))], and the outliers < [Q1 − 1.5 × (Q3 - Q1)] or > [Q3 + 1.5 × (Q3 - Q1)]. (**F**), representative confusion matrices and receiver operating characteristic (ROC) curves from SVM models obtained with the seven serum biomarkers for the classification of AD and other neurodegenerative diseases, including PD, frontotemporal dementia, dementia with Lewy bodies, and progressive supranuclear palsy. ROC curves were compared to the chance levels (dotted lines). $^{***}P < 0.001$; $^{*}P < 0.05$.

4. Discussion

AD is a progressive and devastating neurodegenerative disorder with complex and heterogeneous pathophysiology. Interestingly, accumulating scientific evidence suggests that pathological changes in AD are identical to the autoimmune-driven self-sustaining inflammatory process that originate from prolonged oxidative stress and systemic immune dyshomeostasis (Newcombe et al., 2018; Wu et al., 2021). In compromised immune self-tolerance cases, such as the BBB dysfunction that allows the brain macromolecules from damaged neurons or denatured proteins to interface directly with circulating lymphocytes, the immune system mounts an adaptive response by amplifying certain antibodies that recognize self-antigens and is believed to be a rich source of protein biomarkers. Additionally, by binding to self-antigens with high affinity, autoantibodies initiate and maintain the inflammatory cascade responsible for tissue injuries, which leads to self-destructive, disease-specific autoimmune responses. Autoantibodies can serve as a reflection of brain injury, provide additional diagnostic and targeted therapeutic benefits. Moreover, considerable evidence has shown that immune responses in the central and peripheral systems may undergo significant dynamic changes and exert various heterogeneous effects at different stages of the disease (Bettcher et al., 2021). However, the mechanism and extent to which the different immune components crosstalk and contribute to the disease is a subject that requires more research. Studies have also indicated that peripheral biomolecules, which are modified in unusual ways in various disease states, might involve primary autoantigens that trigger the earliest and most disease-specific autoimmune responses (Reddy et al., 2011), implying that systemic immune signals might originate outside the brain. In this study, we identified seven candidate AD-specific autoantibodies, established a classification model with high accuracy after systemic verification, and optimized the combination, further demonstrating that autoimmunity might specifically reflect the brain changes in AD.

Interestingly, we identified tau as one of the seven candidate proteins, suggesting that anti-tau antibodies might play a role in AD development. Additionally, immunotherapies targeting pathological tau have been tested in several transgenic mouse models of AD, and some have entered clinical trials using different p-tau peptides and antibodies, with some demonstrating great potential (Boutajangout and Wisniewski, 2014; Dai et al., 2018; Dai et al., 2017; Gallardo and Holtzman, 2017;

Wang et al., 2012). However, we have a long way to go to clarify the mechanisms involved in tau immunotherapies (Congdon and Sigurdsson, 2018; Sandusky-Beltran and Sigurdsson, 2020) due to various existing posttranslational modifications, all of which can be potential targeting epitopes. The other six autoantibodies have rarely been reported in AD. SERF1A can act as a regulator of age-related proteotoxicity and drive amyloid formation through charge complementation (Pras et al., 2021; van Ham et al., 2010); CDKN1A is upregulated by Aβ plaque-associated oligodendrocyte progenitor cells that exhibit a senescence-like phenotype in the brains of patients with AD and that of AD mouse models (Elkahloun and Saavedra, 2020; Leandro et al., 2013; Zhang et al., 2019); AGER is considered to contribute to the pathogenesis of AD by mediating Aβ accumulation, mitochondrial damage, and neuro-inflammation (Fang et al., 2010; Son et al., 2017); DNAJC8 had a unique protective role against the aggregation of expanded polyQ-containing proteins such as pathogenic spinocerebellar ataxin-3 proteins in a J-domain independent manner (Ito et al., 2016); Study by DeMarshall et al. demonstrated that a panel of blood-based autoantibodies could be used as diagnostic screener for detecting AD-related pathology, including anti-DNAJC8 autoantibody (DeMarshall et al., 2023). Our results enrich the spectrum of peripheral blood biomarkers and also propose that there might be several significant changes in multiple immunological processes that jointly reflect brain injuries in AD. Furthermore, as a potential assistant screening method, the seven autoantibody biomarkers we identified may complement existing blood indicators, and our autoantibody system can be further optimized.

We analyzed the relationship between the seven serum autoantibodies and the core biomarkers in the CSF of patients with AD in Cohort 2 to verify the diagnostic consistency. Notably, the combined effect of the seven biomarkers in predicting cognitive decline is out-performed concentrations of classic amyloid and tau. This can help identify individuals with normal versus abnormal cognitive function, which is particularly important in patients with cognitive complaints who are non-demented. Additionally, a negative linear relationship between the model evaluation score and cognitive function supported by the rank-transformed model was observed, also indicating that the assay panel can monitor disease severity dynamically. This benefit is also critical because of insufficient cost-effective and minimally invasive methods for the dynamic assessment of AD. Intriguingly, the seven blood-borne autoantibodies also enabled MCI identification, driven by the early stages of AD pathology from the healthy controls in Cohort 3, which is also necessary for early diagnosis and intervention to delay AD progression. We also included other neurodegenerative disorders in Cohort 4 since identifying neurodegenerative diseases is difficult due to clinical heterogeneity. Importantly, except for their potential ability to distinguish AD from cognitive normal controls, the seven autoantibodies could differentiate AD from other neurodegenerative disorders, including PD, DLB, and FTD, further indicating that the seven autoantibodies were specific to AD. Moreover, the results of the different cohorts were consistent, indicating the good repeatability of this detection method. Therefore, the seven autoantibodies have the potential to serve as new peripheral biomarkers for AD. Indeed, as the new surge in neurological diseases associated with various biomarkers of blood-borne autoantibodies, the peripheral autoantibody biomarkers accompanied by AD should not be overlooked (Cao and Zheng, 2018). Aging, as the most significant risk factor for AD, exerts profound impacts on the immune system through inflammaging, immune cell skewing, and diminished youth factors (Franceschi et al., 2018). Considering the heterogeneity and complexity of AD etiology, it is also difficult to comprehensively reflect pathological changes and disease diagnosis using a single biomarker. Multiple immune factors might jointly reflect different aspects of ongoing AD process, which might also be the reason for the significantly improved joint efficiency of the seven indicators.

Therefore, uncovering putative autoimmune components may be crucial in developing new concepts for the pathogenesis, diagnosis, and therapy of AD. To our knowledge, this is the first large study to specifically observe serum autoantibodies in individuals with AD at different stages, other neurodegenerative disorders, and in healthy controls. However, we also have several limitations. Firstly, as the symptoms of MCI patients were mild, most of them were unwilling to perform lumbar puncture, but all of them carried at least one *APOE ε4* allele, and they were diagnosed based on clinical criteria (Albert et al., 2011) but not the ATN framework. Secondly, there was not a standardized criteria to define AD pathology within cohorts. Thirdly, healthy controls or other neurodegenerative patients were not evaluated in having AD pathology or not. Fourth, further validation of the robustness, accuracy, and reproducibility of large ethnically diverse cohorts from multiple centers with longitudinal follow-ups establishing multiperiod data and also cellular and animal model studies of the seven biomarkers are critical for providing insights into the mechanism of AD progression and assessing their potential as therapeutic targets.

Together, AD development is associated with an important serum autoantibody response. We identified seven serum autoantibody biomarkers, which can reflect AD brain injury, clinically delineate discrete disease stages along the MCI-to-AD continuum, and differentiate AD from other neurodegenerative disorders, collectively emphasizing the dynamic role of brain-extrinsic and peripheral signals in the degenerative processes of AD. Therefore, future studies could optimize its application as a convenient biomarker for the early detection and dynamic monitoring of patients with AD.

Declaration of competing interest

The authors declare that they have no known competing financial interests or personal relationships that could have appeared to influence the work reported in this paper.

Data availability

All data are available in the main text or the supplementary materials and from the corresponding author upon request.

Acknowledgments and Disclosures

We are grateful to all participants in the present study.

This work was supported by the National Natural Science Foundation of China (Grant Nos. U22A20300, 81971029, 81501110, 82071216 [to, LS, LS, LF, BJ respectively]), the National Key R&D Program of China (Grant No. 2020YFC2008500 [to LS]), STI2030-Major Projects (Grant No. 2021ZD0201803 [to LS]) and the Hu-Xiang Youth Project (Grant No. 2021RC3028 [to BJ]).

Author contributions

LS designed the study. LF, BJ, XL, HZ, XX, JG and LS collected the samples and performed the clinical evaluation. LF, BJ, HZ, XX and LC performed the experiments. LF, JB, PY, and ZW analyzed the data. LF, BJ, and PY wrote the paper. BT and LS supervised all phases of the project.

Appendix A. Supplementary data

Supplementary data to this article can be found online at https://doi.org/10.1016/j.bbi.2023.11.018.

References

Afzal, S., Bojesen, S.E., Nordestgaard, B.G., 2014. Reduced 25-hydroxyvitamin D and risk of Alzheimer's disease and vascular dementia. Alzheimers Dement. 10, 296–302.

Albert, M.S., DeKosky, S.T., Dickson, D., Dubois, B., Feldman, H.H., Fox, N.C., Gamst, A., Holtzman, D.M., Jagust, W.J., Petersen, R.C., Snyder, P.J., Carrillo, M.C., Thies, B., Phelps, C.H., 2011. The diagnosis of mild cognitive impairment due to Alzheimer's disease: recommendations from the National Institute on Aging-Alzheimer's

Association workgroups on diagnostic guidelines for Alzheimer's disease. Alzheimers Dement. 7, 270–279.
Angelucci, F., Cechova, K., Amlerova, J., Hort, J., 2019. Antibiotics, gut microbiota, and Alzheimer's disease. J. Neuroinflamm. 16, 108.
Ashton, N.J., Pascoal, T.A., Karikari, T.K., Benedet, A.L., Lantero-Rodriguez, J., Brinkmalm, G., Snellman, A., Schöll, M., Troakes, C., Hye, A., Gauthier, S., Vanmechelen, E., Zetterberg, H., Rosa-Neto, P., Blennow, K., 2021. Plasma p-tau231: a new biomarker for incipient Alzheimer's disease pathology. Acta Neuropathol. 141, 709–724.
Bayoumy, S., Verberk, I.M.W., den Dulk, B., Hussainali, Z., Zwan, M., van der Flier, W. M., Ashton, N.J., Zetterberg, H., Blennow, K., Vanbrabant, J., Stoops, E., Vanmechelen, E., Dage, J.L., Teunissen, C.E., 2021. Clinical and analytical comparison of six Simoa assays for plasma P-tau isoforms P-tau181, P-tau217, and P-tau231. Alzheimers Res. Ther. 13, 198.
Bettcher, B.M., Tansey, M.G., Dorothée, G., Heneka, M.T., 2021. Peripheral and central immune system crosstalk in Alzheimer disease - a research prospectus. Nat. Rev. Neurol. 17, 689–701.
Boutajangout, A., Wisniewski, T., 2014. Tau-based therapeutic approaches for Alzheimer's disease - a mini-review. Gerontology 60, 381–385.
Cao, W., Zheng, H., 2018. Peripheral immune system in aging and Alzheimer's disease. Mol. Neurodegener. 13, 51.
Chatterjee, P., Pedrini, S., Ashton, N.J., Tegg, M., Goozee, K., Singh, A.K., Karikari, T.K., Simrén, J., Vanmechelen, E., Armstrong, N.J., Hone, E., Asih, P.R., Taddei, K., Doré, V., Villemagne, V.L., Sohrabi, H.R., Zetterberg, H., Masters, C.L., Blennow, K., Martins, R.N., 2022. Diagnostic and prognostic plasma biomarkers for preclinical Alzheimer's disease. Alzheimers Dement. 18, 1141–1154.
Congdon, E.E., Sigurdsson, E.M., 2018. Tau-targeting therapies for Alzheimer disease. Nat. Rev. Neurol. 14, 399–415.
Dai, C.L., Tung, Y.C., Liu, F., Gong, C.X., Iqbal, K., 2017. Tau passive immunization inhibits not only tau but also Aβ pathology. Alzheimers Res. Ther. 9, 1.
Dai, C.L., Hu, W., Tung, Y.C., Liu, F., Gong, C.X., Iqbal, K., 2018. Tau passive immunization blocks seeding and spread of Alzheimer hyperphosphorylated Tau-induced pathology in 3 × Tg-AD mice. Alzheimers Res. Ther. 10, 13.
Daniilidou, M., Tsolaki, M., Giannakouros, T., Nikolakaki, E., 2011. Detection of elevated antibodies against SR protein kinase 1 in the serum of Alzheimer's disease patients. J. Neuroimmunol. 238, 67–72.
DeMarshall, C.A., Viviano, J., Emrani, S., Thayasivam, U., Godsey, G.A., Sarkar, A., Belinka, B., Libon, D.J., Nagele, R.G., 2023. Early detection of Alzheimer's disease-related pathology using a multi-disease diagnostic platform employing autoantibodies as blood-based biomarkers. J. Alzheimers Dis. 92, 1077–1091.
Elkahloun, A.G., Saavedra, J.M., 2020. Candesartan neuroprotection in rat primary neurons negatively correlates with aging and senescence: a transcriptomic analysis. Mol. Neurobiol. 57, 1656–1673.
Fang, F., Lue, L.F., Yan, S., Xu, H., Luddy, J.S., Chen, D., Walker, D.G., Stern, D.M., Yan, S., Schmidt, A.M., Chen, J.X., Yan, S.S., 2010. RAGE-dependent signaling in microglia contributes to neuroinflammation, Abeta accumulation, and impaired learning/memory in a mouse model of Alzheimer's disease. FASEB J. 24, 1043–1055.
Ferrari, C., Sorbi, S., 2021. The complexity of Alzheimer's disease: an evolving puzzle. Physiol. Rev. 101, 1047–1081.
Franceschi, C., Garagnani, P., Parini, P., Giuliani, C., Santoro, A., 2018. Inflammaging: a new immune-metabolic viewpoint for age-related diseases. Nat. Rev. Endocrinol. 14, 576–590.
Gallardo, G., Holtzman, D.M., 2017. Antibody Therapeutics Targeting Aβ and Tau. Cold Spring Harb. Perspect. Med. 7.
GBD 2019 Dementia Forecasting Collaborators. 2022. Estimation of the global prevalence ofdementia in 2019 and forecasted prevalence in 2050: an analysis for the Global Burden of Disease Study 2019.Lancet Public Health 7,e105-e125.
Höglinger, G.U., Respondek, G., Stamelou, M., Kurz, C., Josephs, K.A., Lang, A.E., Mollenhauer, B., Müller, U., Nilsson, C., Whitwell, J.L., Arzberger, T., Englund, E., Gelpi, E., Giese, A., Irwin, D.J., Meissner, W.G., Pantelyat, A., Rajput, A., van Swieten, J.C., Troakes, C., Antonini, A., Bhatia, K.P., Bordelon, Y., Compta, Y., Corvol, J.C., Colosimo, C., Dickson, D.W., Dodel, R., Ferguson, L., Grossman, M., Kassubek, J., Krismer, F., Levin, J., Lorenzl, S., Morris, H.R., Nestor, P., Oertel, W.H., Poewe, W., Rabinovici, G., Rowe, J.B., Schellenberg, G.D., Seppi, K., van Eimeren, T., Wenning, G.K., Boxer, A.L., Golbe, L.I., Litvan, I., 2017. Clinical diagnosis of progressive supranuclear palsy: The movement disorder society criteria. Mov. Disord. 32, 853–864.
Huang, Z., Wong, L.W., Su, Y., Huang, X., Wang, N., Chen, H., Yi, C., 2020. Blood-brain barrier integrity in the pathogenesis of Alzheimer's disease. Front. Neuroendocrinol. 59, 100857.
Illán-Gala, I., Lleo, A., Karydas, A., Staffaroni, A.M., Zetterberg, H., Sivasankaran, R., Grinberg, L.T., Spina, S., Kramer, J.H., Ramos, E.M., Coppola, G., La Joie, R., Rabinovici, G.D., Perry, D.C., Gorno-Tempini, M.L., Seeley, W.W., Miller, B.L., Rosen, H.J., Blennow, K., Boxer, A.L., Rojas, J.C., 2021. Plasma tau and neurofilament light in frontotemporal lobar degeneration and Alzheimer disease. Neurology 96, e671–e683.
Ito, N., Kamiguchi, K., Nakanishi, K., Sokolovskya, A., Hirohashi, Y., Tamura, Y., Murai, A., Yamamoto, E., Kanaseki, T., Tsukahara, T., Kochin, V., Chiba, S., Shimohama, S., Sato, N., Torigoe, T., 2016. A novel nuclear DnaJ protein, DNAJC8, can suppress the formation of spinocerebellar ataxia 3 polyglutamine aggregation in a J-domain independent manner. Biochem. Biophys. Res. Commun. 474, 626–633.
Jack Jr., C.R., Bennett, D.A., Blennow, K., Carrillo, M.C., Dunn, B., Haeberlein, S.B., Holtzman, D.M., Jagust, W., Jessen, F., Karlawish, J., Liu, E., Molinuevo, J.L., Montine, T., Phelps, C., Rankin, K.P., Rowe, C.C., Scheltens, P., Siemers, E., Snyder, H.M., Sperling, R., 2018. NIA-AA Research Framework: Toward a biological definition of Alzheimer's disease. Alzheimers Dement. 14, 535–562.
Jiao, B., Liu, X., Tang, B., Hou, L., Zhou, L., Zhang, F., Zhou, Y., Guo, J., Yan, X., Shen, L., 2014. Investigation of TREM2, PLD3, and UNC5C variants in patients with Alzheimer's disease from mainland China. Neurobiol. Aging 35, 2422.e2429-2422.e2411.
Jiao, B., Liu, H., Guo, L., Xiao, X., Liao, X., Zhou, Y., Weng, L., Zhou, L., Wang, X., Jiang, Y., Yang, Q., Zhu, Y., Zhou, L., Zhang, W., Wang, J., Yan, X., Li, J., Tang, B., Shen, L., 2021. The role of genetics in neurodegenerative dementia: a large cohort study in South China. NPJ Genom. Med. 6, 69.
Leandro, G.S., Lobo, R.R., Oliveira, D.V., Moriguti, J.C., Sakamoto-Hojo, E.T., 2013. Lymphocytes of patients with Alzheimer's disease display different DNA damage repair kinetics and expression profiles of DNA repair and stress response genes. Int. J. Mol. Sci. 14, 12380–12400.
Li, Y., Macyczko, J.R., Liu, C.C., Bu, G., 2022. ApoE4 reduction: An emerging and promising therapeutic strategy for Alzheimer's disease. Neurobiol. Aging 115, 20–28.
Lopresti, B.J., Klunk, W.E., Mathis, C.A., Hoge, J.A., Ziolko, S.K., Lu, X., Meltzer, C.C., Schimmel, K., Tsopelas, N.D., DeKosky, S.T., Price, J.C., 2005. Simplified quantification of Pittsburgh Compound B amyloid imaging PET studies: a comparative analysis. J. Nucl. Med. 46, 1959–1972.
McKeith, I.G., Dickson, D.W., Lowe, J., Emre, M., O'Brien, J.T., Feldman, H., Cummings, J., Duda, J.E., Lippa, C., Perry, E.K., Aarsland, D., Arai, H., Ballard, C.G., Boeve, B., Burn, D.J., Costa, D., Del Ser, T., Dubois, B., Galasko, D., Gauthier, S., Goetz, C.G., Gomez-Tortosa, E., Halliday, G., Hansen, L.A., Hardy, J., Iwatsubo, T., Kalaria, R.N., Kaufer, D., Kenny, R.A., Korczyn, A., Kosaka, K., Lee, V.M., Lees, A., Litvan, I., Londos, E., Lopez, O.L., Minoshima, S., Mizuno, Y., Molina, J.A., Mukaetova-Ladinska, E.B., Pasquier, F., Perry, R.H., Schulz, J.B., Trojanowski, J.Q., Yamada, M., 2005. Diagnosis and management of dementia with Lewy bodies: third report of the DLB Consortium. Neurology 65, 1863–1872.
McKhann, G.M., Knopman, D.S., Chertkow, H., Hyman, B.T., Jack Jr., C.R., Kawas, C.H., Klunk, W.E., Koroshetz, W.J., Manly, J.J., Mayeux, R., Mohs, R.C., Morris, J.C., Rossor, M.N., Scheltens, P., Carrillo, M.C., Thies, B., Weintraub, S., Phelps, C.H., 2011. The diagnosis of dementia due to Alzheimer's disease: recommendations from the National Institute on Aging-Alzheimer's Association workgroups on diagnostic guidelines for Alzheimer's disease. Alzheimers Dement. 7, 263–269.
Minoshima, S., Drzezga, A.E., Barthel, H., Bohnen, N., Djekidel, M., Lewis, D.H., Mathis, C.A., McConathy, J., Nordberg, A., Sabri, O., Seibyl, J.P., Stokes, M.K., Van Laere, K., 2016. SNMMI procedure standard/EANM practice guideline for amyloid PET imaging of the brain 1.0. J. Nucl. Med. 57, 1316–1322.
Nakamura, A., Kaneko, N., Villemagne, V.L., Kato, T., Doecke, J., Doré, V., Fowler, C., Li, Q.X., Martins, R., Rowe, C., Tomita, T., Matsuzaki, K., Ishii, K., Ishii, K., Arahata, Y., Iwamoto, S., Ito, K., Tanaka, K., Masters, C.L., Yanagisawa, K., 2018. High performance plasma amyloid-β biomarkers for Alzheimer's disease. Nature 554, 249–254.
Newcombe, E.A., Camats-Perna, J., Silva, M.L., Valmas, N., Huat, T.J., Medeiros, R., 2018. Inflammation: the link between comorbidities, genetics, and Alzheimer's disease. J. Neuroinflammation 15, 276.
Nourhashemi, F., Hooper, C., Cantet, C., Féart, C., Gennero, I., Payoux, P., Salabert, A.S., Guyonnet, S., De Souto Barreto, P., Vellas, B., 2018. Cross-sectional associations of plasma vitamin D with cerebral β-amyloid in older adults at risk of dementia. Alzheimers Res. Ther. 10, 43.
Postuma, R.B., Berg, D., Stern, M., Poewe, W., Olanow, C.W., Oertel, W., Obeso, J., Marek, K., Litvan, I., Lang, A.E., Halliday, G., Goetz, C.G., Gasser, T., Dubois, B., Chan, P., Bloem, B.R., Adler, C.H., Deuschl, G., 2015. MDS clinical diagnostic criteria for Parkinson's disease. Mov. Disord. 30, 1591–1601.
Pras, A., Houben, B., Aprile, F.A., Seinstra, R., Gallardo, R., Janssen, L., Hogewerf, W., Gallrein, C., De Vleeschouwer, M., Mata-Cabana, A., Koopman, M., Stroo, E., de Vries, M., Louise Edwards, S., Kirstein, J., Vendruscolo, M., Falsone, S.F., Rousseau, F., Schymkowitz, J., Nollen, E.A.A., 2021. The cellular modifier MOAG-4/SERF drives amyloid formation through charge complementation. EMBO J. 40, e107568.
Preische, O., Schultz, S.A., Apel, A., Kuhle, J., Kaeser, S.A., Barro, C., Gräber, S., Kuder-Buletta, E., LaFougere, C., Laske, C., Vöglein, J., Levin, J., Masters, C.L., Martins, R., Schofield, P.R., Rossor, M.N., Graff-Radford, N.R., Salloway, S., Ghetti, B., Ringman, J.M., Noble, J.M., Chhatwal, J., Goate, A.M., Benzinger, T.L.S., Morris, J. C., Bateman, R.J., Wang, G., Fagan, A.M., McDade, E.M., Gordon, B.A., Jucker, M., 2019. Serum neurofilament dynamics predicts neurodegeneration and clinical progression in presymptomatic Alzheimer's disease. Nat. Med. 25, 277–283.
Rascovsky, K., Hodges, J.R., Knopman, D., Mendez, M.F., Kramer, J.H., Neuhaus, J., van Swieten, J.C., Seelaar, H., Dopper, E.G., Onyike, C.U., Hillis, A.E., Josephs, K.A., Boeve, B.F., Kertesz, A., Seeley, W.W., Rankin, K.P., Johnson, J.K., Gorno-Tempini, M.L., Rosen, H., Prioleau-Latham, C.E., Lee, A., Kipps, C.M., Lillo, P., Piguet, O., Rohrer, J.D., Rossor, M.N., Warren, J.D., Fox, N.C., Galasko, D., Salmon, D.P., Black, S.E., Mesulam, M., Weintraub, S., Dickerson, B.C., Diehl-Schmid, J., Pasquier, F., Deramecourt, V., Lebert, F., Pijnenburg, Y., Chow, T.W., Manes, F., Grafman, J., Cappa, S.F., Freedman, M., Grossman, M., Miller, B.L., 2011. Sensitivity of revised diagnostic criteria for the behavioural variant of frontotemporal dementia. Brain 134, 2456–2477.
Reddy, M.M., Wilson, R., Wilson, J., Connell, S., Gocke, A., Hynan, L., German, D., Kodadek, T., 2011. Identification of candidate IgG biomarkers for Alzheimer's disease via combinatorial library screening. Cell 144, 132–142.
Sabatino Jr., J.J., Pröbstel, A.K., Zamvil, S.S., 2019. B cells in autoimmune and neurodegenerative central nervous system diseases. Nat. Rev. Neurosci. 20, 728–745.

Sadick, J.S., O'Dea, M.R., Hasel, P., Dykstra, T., Faustin, A., Liddelow, S.A., 2022. Astrocytes and oligodendrocytes undergo subtype-specific transcriptional changes in Alzheimer's disease. Neuron 110, 1788–1805.e1710.
San Segundo-Acosta, P., Montero-Calle, A., Fuentes, M., Rábano, A., Villalba, M., Barderas, R., 2019. Identification of Alzheimer's Disease Autoantibodies and Their Target Biomarkers by Phage Microarrays. J. Proteome Res. 18, 2940–2953.
San Segundo-Acosta, P., Montero-Calle, A., Jernbom-Falk, A., Alonso-Navarro, M., Pin, E., Andersson, E., Hellström, C., Sánchez-Martínez, M., Rábano, A., Solís-Fernández, G., Peláez-García, A., Martínez-Useros, J., Fernández-Aceñero, M.J., Månberg, A., Nilsson, P., Barderas, R., 2021. Multiomics Profiling of Alzheimer's disease serum for the identification of autoantibody biomarkers. J. Proteome Res. 20, 5115–5130.
Sandusky-Beltran, L.A., Sigurdsson, E.M., 2020. Tau immunotherapies: Lessons learned, current status and future considerations. Neuropharmacology 175, 108104.
Scheltens, P., De Strooper, B., Kivipelto, M., Holstege, H., Chételat, G., Teunissen, C.E., Cummings, J., van der Flier, W.M., 2021. Alzheimer's disease. Lancet 397, 1577–1590.
Seeburger, J.L., Holder, D.J., Combrinck, M., Joachim, C., Laterza, O., Tanen, M., Dallob, A., Chappell, D., Snyder, K., Flynn, M., Simon, A., Modur, V., Potter, W.Z., Wilcock, G., Savage, M.J., Smith, A.D., 2015. Cerebrospinal fluid biomarkers distinguish postmortem-confirmed Alzheimer's disease from other dementias and healthy controls in the OPTIMA cohort. J. Alzheimers Dis. 44, 525–539.
Son, M., Oh, S., Park, H., Ahn, H., Choi, J., Kim, H., Lee, H.S., Lee, S., Park, H.J., Kim, S. U., Lee, B., Byun, K., 2017. Protection against RAGE-mediated neuronal cell death by sRAGE-secreting human mesenchymal stem cells in 5xFAD transgenic mouse model. Brain Behav. Immun. 66, 347–358.
Sorboni, S.G., Moghaddam, H.S., Jafarzadeh-Esfehani, R., Soleimanpour, S., 2022. A comprehensive review on the role of the gut microbiome in human neurological disorders. Clin. Microbiol. Rev. 35, e0033820.
Teunissen, C.E., Petzold, A., Bennett, J.L., Berven, F.S., Brundin, L., Comabella, M., Franciotta, D., Frederiksen, J.L., Fleming, J.O., Furlan, R., Hintzen, R.Q., Hughes, S. G., Johnson, M.H., Krasulova, E., Kuhle, J., Magnone, M.C., Rajda, C., Rejdak, K., Schmidt, H.K., van Pesch, V., Waubant, E., Wolf, C., Giovannoni, G., Hemmer, B., Tumani, H., Deisenhammer, F., 2009. A consensus protocol for the standardization of cerebrospinal fluid collection and biobanking. Neurology 73, 1914–1922.
van Ham, T.J., Holmberg, M.A., van der Goot, A.T., Teuling, E., Garcia-Arencibia, M., Kim, H.E., Du, D., Thijssen, K.L., Wiersma, M., Burggraaff, R., van Bergeijk, P., van Rheenen, J., Jerre van Veluw, G., Hofstra, R.M., Rubinsztein, D.C., Nollen, E.A., 2010. Identification of MOAG-4/SERF as a regulator of age-related proteotoxicity. Cell 142, 601–612.
Wang, W., Fan, L., Xu, D., Wen, Z., Yu, R., Ma, Q., 2012. Immunotherapy for Alzheimer's disease. Acta Biochim. Biophys. Sin. (Shanghai) 44, 807–814.
Wang, B.Z., Zailan, F.Z., Wong, B.Y.X., Ng, K.P., Kandiah, N., 2020. Identification of novel candidate autoantibodies in Alzheimer's disease. Eur. J. Neurol. 27, 2292–2296.
Wu, K.M., Zhang, Y.R., Huang, Y.Y., Dong, Q., Tan, L., Yu, J.T., 2021. The role of the immune system in Alzheimer's disease. Ageing Res. Rev. 70, 101409.
Yarchoan, M., Xie, S.X., Kling, M.A., Toledo, J.B., Wolk, D.A., Lee, E.B., Van Deerlin, V., Lee, V.M., Trojanowski, J.Q., Arnold, S.E., 2012. Cerebrovascular atherosclerosis correlates with Alzheimer pathology in neurodegenerative dementias. Brain 135, 3749–3756.
Zhang, P., Kishimoto, Y., Grammatikakis, I., Gottimukkala, K., Cutler, R.G., Zhang, S., Abdelmohsen, K., Bohr, V.A., Misra Sen, J., Gorospe, M., Mattson, M.P., 2019. Senolytic therapy alleviates Aβ-associated oligodendrocyte progenitor cell senescence and cognitive deficits in an Alzheimer's disease model. Nat. Neurosci. 22, 719–728.
Zlokovic, B.V., 2011. Neurovascular pathways to neurodegeneration in Alzheimer's disease and other disorders. Nat. Rev. Neurosci. 12, 723–738.